Novel Superconductivity in Metallic SnH_4 under High Pressure

J. S. Tse,[*,†] Y. Yao,[*,‡] and K. Tanaka

Department of Physics and Engineering Physics, University of Saskatchewan, Saskatoon, Canada, S7N 5E2

(Received 1 August 2006; published 15 March 2007)

From first-principles calculations, a high-pressure metallic phase of SnH_4 with a novel layered structure intercalated by "H_2" units is revealed. This structure is stable at pressure between 70 and 160 GPa. A remarkable feature of this structure is the presence of soft modes in the phonon band structure induced by Fermi surface nesting and Kohn anomalies that lead to very strong electron-phonon coupling. The application of the Allen-Dynes modified McMillan equation with the calculated electron-phonon coupling parameter λ shows that a superconducting critical temperature close to 80 K can be achieved at 120 GPa.

DOI: 10.1103/PhysRevLett.98.117004 PACS numbers: 74.70.Ad, 74.10.+v, 74.25.Jb, 74.62.Fj

Since the prediction of possible high-T_c superconductivity in solid hydrogen at very high pressure [1,2], despite intense experimental efforts, the observation of metallic H_2 in the solid phase remains elusive. Recently, it was suggested that dense hydrogen-dominated metallic alloys, in strongly compressed Group IV hydrides, can be potential candidate materials for a high-T_c superconductor [3,4]. Since then, several experimental and theoretical investigations, mainly focused on SiH_4, have been undertaken to investigate this prediction [5–7]. No study on the hydrides of heavier group IV elements such as SnH_4 has been attempted. SnH_4 offers several potential advantages over SiH_4. The heavier Sn atom will yield lower energy vibrations that help mediate electron-phonon coupling (EPC). A weaker Sn-H bond enthalpy may facilitate complete dissociation of the Sn-H bonds at lower pressure. To investigate these possibilities, first-principles calculations have been performed to characterize the high-pressure structure and potential superconducting property of SnH_4. The computational studies reveal a high-pressure superconducting phase of SnH_4 which is stable between 70 GPa and 160 GPa with a predicted T_c close to 80 K at 120 GPa.

In the absence of the knowledge of high-pressure SnH_4 structure, the starting point of this investigation was initiated with the *Ccca* structure reported earlier [7] for the high-pressure phase of SiH_4. A series of simulated annealing and geometry optimization revealed a metallic $P6/mmm$ structure [Fig. 1(a)] with the primitive unit cell containing only a single SnH_4 unit [8]. Between 70 to 160 GPa, this structure has the lowest energy among several competing structures; therefore, it is the most favored structure. The Sn atom occupies the crystallographic 1*a* site and the H atoms are on the 4*h* sites. The Sn atoms are arranged in 2D close-packed hexagonal layers. The in-plane Sn-Sn bond length varies from 3.189 Å to 2.961 Å from 70 GPa to 160 GPa. In this pressure range, adjacent Sn layers are bridged by a pair of H atoms with a Sn-H bond length from 2.129 Å to 1.962 Å. The most striking feature of this structure is the exceptionally short H-H contact from 0.845 Å to 0.841 Å from 70 GPa to 160 GPa. The analysis of the electron localization function (ELF) [14] [Fig. 1(a)] shows a very high value (close to 1) in regions between the 2 H atoms. The strong electron localization between the 2 H atoms indicates pairing of electrons from the H atoms. As will be described later, interactions of these novel "H_2" units with the Sn framework contribute significantly to the EPC mechanism. The ELF values in the region connecting the adjacent Sn layers are close to 0.6, suggesting weak covalent bonding.

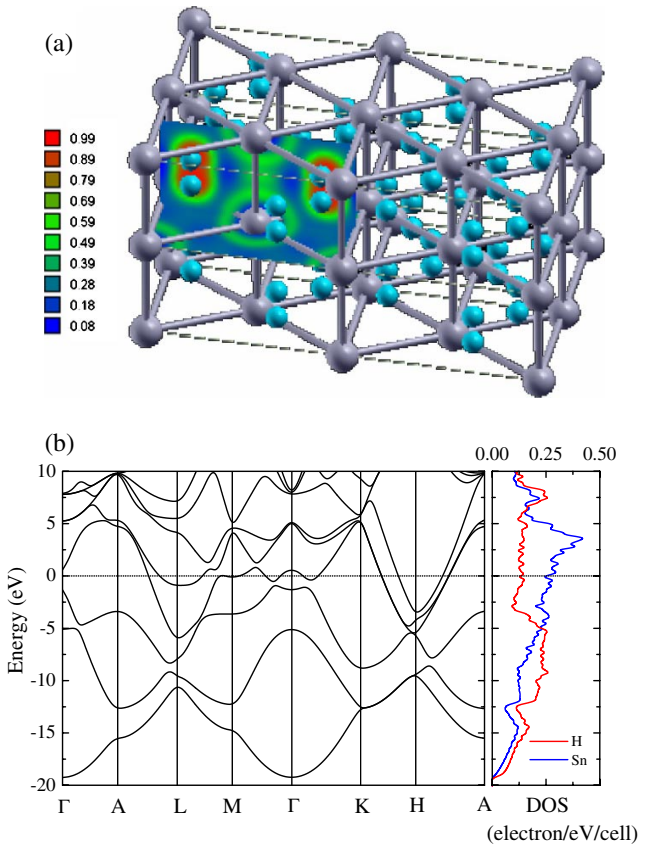

FIG. 1 (color online). (a) The crystal structure of $P6/mmm$ SnH_4 calculated at 120 GPa with the ELF shown in the (100) plane. (b) The electronic band structure and projected DOS of $P6/mmm$ SnH_4 calculated at 120 GPa.

The electronic band structure [15], density of electronic states (DOS), vibrational properties, and EPC have been computed at 70, 120, and 160 GPa. The results were found to be similar for different pressures and details are reported here only for the intermediate pressure phase at 120 GPa. The electronic band structure and DOS at 120 GPa are demonstrated in Fig. 1(b). The DOS shows significant overlap between the orbitals of Sn and H atoms. The calculated valence bandwidth is about 19.5 eV, consistent with the prediction made earlier for dense hydrogen alloys [3,4]. The band structure reveals metallic character with large dispersion bands crossing the Fermi level (E_F) and a flat band in the vicinity of E_F close to the M point. The simultaneous occurrence of flat and steep bands near the Fermi level has been suggested as favorable conditions for enhancing electron pairing, which is essential to superconducting behavior [17].

The phonon band structure and the projected DOS at 120 GPa are shown in Fig. 2(a). The absence of imaginary frequency modes indicates that the structure is stable. Additional phonon calculations establish the stability range to be between 70 and 160 GPa. A direct result of this unique H_2 "intercalated layered" structure is that the vibrational modes can be divided into three major regions. Weak interactions between the Sn framework and H atoms are found in the low-energy translational region below 260 cm^{-1}. As will be discussed later, these low-frequency vibrations contribute significantly to the EPC parameter λ. Molecular-like H-H vibrations are observed at high frequencies (2200–2600 cm^{-1}). These almost localized vibrations are the consequence of strong H-H interactions as revealed from the ELF analysis [Fig. 1(b)]. The H . . . Sn . . . H bending vibrations dominate the intermediate-frequency region (500–1400 cm^{-1}).

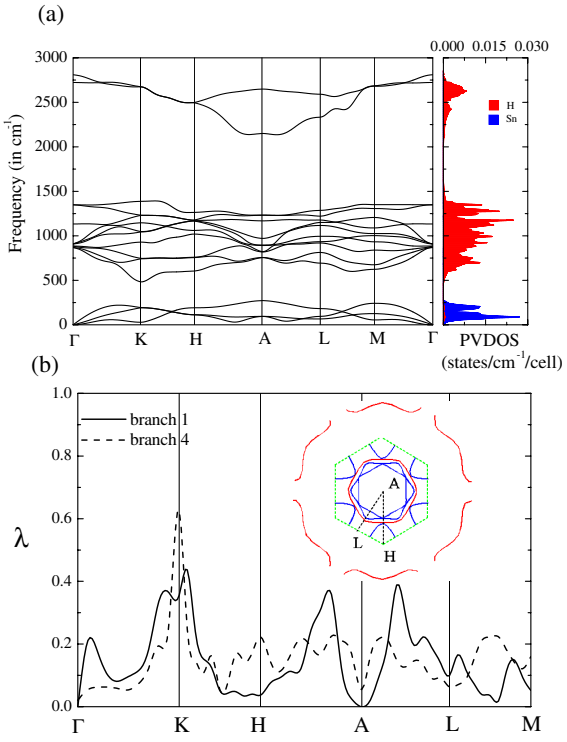

FIG. 2 (color online). (a) The phonon band structure and projected DOS of $P6/mmm$ SnH_4 calculated at 120 GPa. (b) The partial EPC parameters λ in two soft phonon branches (branch 1 and 4). Inset is the (001) cross section of the first $B.Z$ with the boundary represented by green dotted lines. The Fermi surface is resented by blue curves. Red curves correspond to the Kohn anomaly surface.

A striking feature of the phonon band structure is the presence of soft phonon modes, which can be classified into two groups: those induced by Fermi surface (FS) nesting and by Kohn anomalies. The former includes the decreases in the phonon frequency of the lowest acoustic branch (branch 1) observed at the K and M points, as well as the dip in the lowest optical branch (branch 4) at the K point. The second group consists of the two dips in phonon branch 1 along the $H \rightarrow A$ and $A \rightarrow L$ directions [Fig. 2(a)]. Details of the nesting of FS can be analyzed by the nesting function [18,19]

$$\xi(Q) = \frac{1}{N}\sum_k \delta(\varepsilon_k - \varepsilon_F)\delta(\varepsilon_{k+Q} - \varepsilon_F) \propto \oint \frac{d\ell_k}{|\vec{v}_k \times \vec{v}_{k+Q}|}, \quad (1)$$

where the line integral is along the intersection of FS and its image displaced by vector Q, $\vec{v}_k$ is the Fermi velocity, and N the number of k points. (The proportionality is valid only when the two surfaces are not tangential to each other.) The $\xi(Q)$ becomes large when $\vec{v}_k$ and $\vec{v}_{k+Q}$ are small and/or collinear. This concept helps to determine possible nesting vectors from the FS shown in Fig. 3. In the FS of the lowest-energy band crossing the Fermi level [Fig. 3(b)], the electron velocities of the opposite faces of the "hexagonal (sake) cup" shaped portions are parallel to each other. Therefore, FS nesting is expected to occur. Moving downward from the top to the zone center, corresponding nesting vectors span Q points along the $\Gamma \rightarrow M$ and $\Gamma \rightarrow K$ directions. This qualitative description is confirmed by the quantitative calculations presented in Fig. 4(a), where $\xi(Q)$ is shown to be strongest along the $\Gamma \rightarrow M$ and $\Gamma \rightarrow K$ directions. The peak at the K point is facilitated by nesting between two opposite hexagonal faces of the FS of the middle energy band at the top portion of the first BZ [Fig. 3(c)]. The two opposite faces are parallel to each other at the top portion and curved outward toward the edge of the first BZ when moving downward. This band has smaller Fermi velocities that are collinear in the top portion of the FS. In Fig. 4(a), the two peaks in $\xi(Q)$ along the $\Gamma \rightarrow A$ direction are related to nesting vectors along the z axis. Along the $A \rightarrow L$ and $H \rightarrow A$ directions, $\xi(Q)$ features several broad but weak peaks that can be attributed to Kohn anomalies. Kohn anomaly is a special case of FS nesting with a nesting vector of $2k_F$ [inset of Fig. 2(b)], and it induces distinct phonon softening [18,20] in branch 1 along the $H \rightarrow A$ and $A \rightarrow L$ directions. Finally, the decrease in the vibrational frequency of the

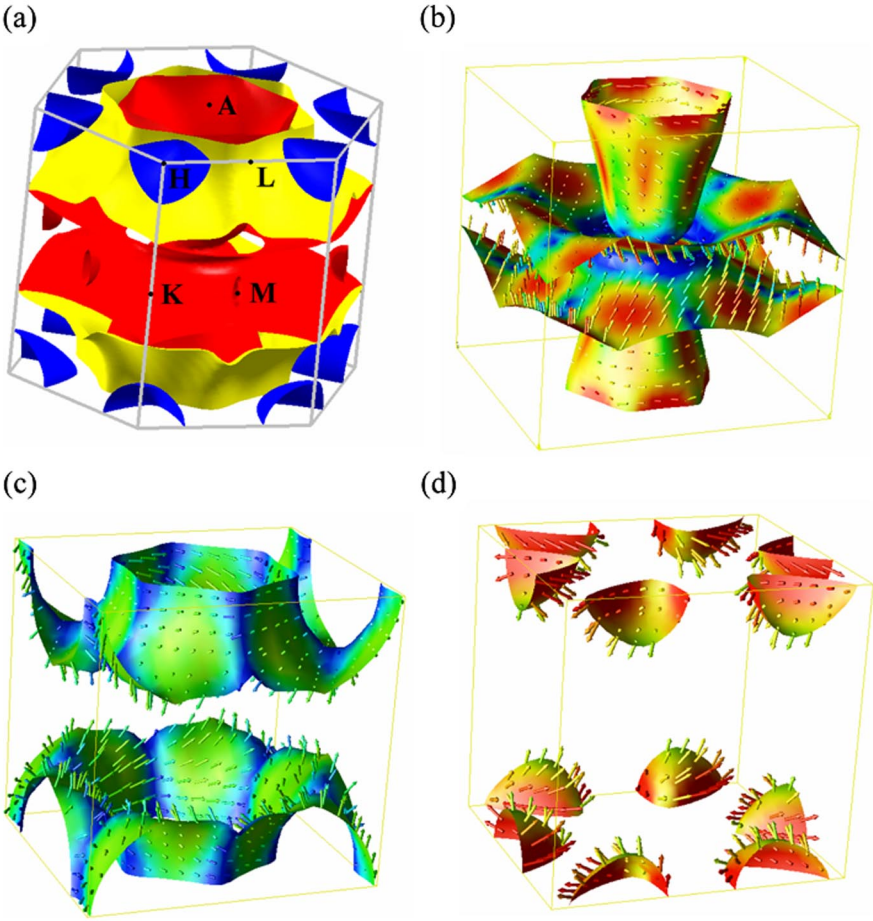

FIG. 3 (color online). The Fermi surface of $P6/mmm$ SnH_4 calculated at 120 GPa. (a) The 3D view of the Fermi surface including all cutting bands. (b)–(d) The Fermi surface of each band colored by the value of the Fermi velocity, with arrows representing the velocity directions. Red color indicates high velocity; blue color denotes low velocity. The Fermi surface is sampled with a $24 \times 24 \times 30$ k mesh.

second highest phonon branch along the $H \rightarrow A \rightarrow L$ direction [Fig. 2(a)] is likely to be a result of phonon renormalization caused by Kohn anomalies [20].

To explore the dependence of the EPC on soft phonon modes, the partial EPC parameter λ for the two softened branches (branch 1 and 4) along several high-symmetry directions is depicted in Fig. 2(b). As results of phonon softening and FS nesting or Kohn anomalies, broad peaks are observed at the k point and along the $H \rightarrow A$ and $A \rightarrow L$ directions. As seen in $\xi(Q)$ [Fig. 4(a)], although FS nesting vectors span Q points along the $\Gamma \rightarrow M$ direction, there is no peak at the M point in the partial EPC parameter λ shown in Fig. 2(b). This feature is a result of smaller magnitudes of the relevant electron-phonon matrix elements. This is substantiated by the fact that in branch 1, the phonon softening at the M point is not as distinct as that at the k point.

To investigate possible superconductivity, phonon linewidths, the EPC parameter λ, and the Eliashberg phonon spectral function $\alpha^2F(\omega)$ [21] have been calculated. The calculated λ is 1.20 at 120 GPa. The spectral function $\alpha^2F(\omega)$ obtained at 120 GPa and the integrated EPC parameter λ as a function of frequency are shown in Fig. 4(b). The integrated λ among the acoustic modes below 260 cm^{-1} constitutes 25% of the total EPC parameter. The intermediate-frequency vibrational modes between 500 cm^{-1} and 1400 cm^{-1} contribute 68% to the total EPC parameter. The remaining 7% of the total EPC parameter is derived from the vibrational modes above 2200 cm^{-1}. The superconducting critical temperature can be estimated from the Allen-Dynes modified McMillan equation [22] $T_c = \frac{\omega_{\log}}{1.2} \exp[-\frac{1.04(1+\lambda)}{\lambda-\mu^*(1+0.62\lambda)}]$, where $\omega_{\log}$ is the logarithmic average frequency and μ^* the Coulomb pseudopotential. This equation has been found to be highly accurate for materials with $\lambda < 1.5$. The $\omega_{\log}$ are calculated directly from the phonon spectrum, and μ^* is often taken as $\sim$0.1 for most metals. At 120 GPa, the calculated $\omega_{\log}$ is 921 K. Using μ^* of 0.1, 0.12, and 0.13, the estimated T_c are 83, 77, and 73 K, respectively. It was proposed earlier [3] that an appropriate value for μ^* for dense metal hydrides is 0.13. In view of the very large predicted λ, the accuracy of the predicted T_c is reexamined, using another modification of the McMillan equation suitable for very strong coupling materials [23]. The resulting T_c is slightly higher by 6%–7%.

To study the pressure dependence of the superconducting critical temperature, the EPC calculations have also been performed at 70 GPa and 160 GPa. The calculated $\omega_{\log}$ at 70, 120, and 160 GPa are 660, 921, and 848 K, and λ 1.30, 1.20, and 1.29, respectively. Interestingly, λ does not show a monotonic increase with pressure and has larger values at 70 and 160 GPa than 120 GPa. This effect is the

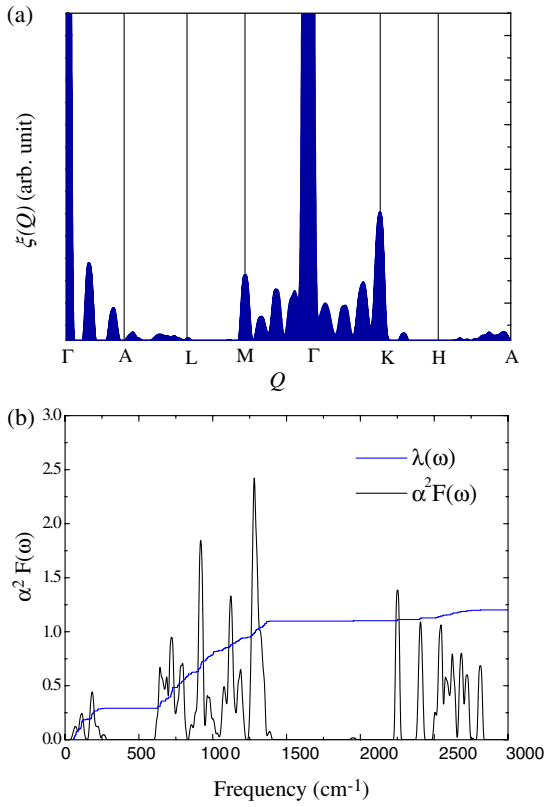

FIG. 4 (color online). (a) The nesting function $\xi(Q)$ of $P6/mmm$ SnH_4 along several high-symmetry lines of Q calculated at 120 GPa. The k points are sampled directly on the Fermi surface and a very strict broadening of 0.01 is used in the Gaussian function to simulate the δ function. The present calculation employs 6830 k points and 141 Q points, which result in the evaluation of energy ε_{k+Q} at 963 030 points. (b) The Eliashberg phonon spectral function $\alpha^2F(\omega)$ and the electron-phonon integral $\lambda(\omega)$ of $P6/mmm$ SnH_4 calculated at 120 GPa.

consequence of a complicated balance between the entire phonon spectrum and the soft phonon modes at different pressures. Using μ^* of 0.13, the estimated T_c are 58, 73, and 74 K at 70, 120, and 150 GPa, respectively. Therefore, between 70 and 120 GPa, the pressure coefficient (dT_c/dP) is about -0.304 K/GPa. The superconducting critical temperature of $P6/mmm$ SnH_4 has only a weak dependence on pressure.

In conclusion, first-principles calculations reveal a novel structure of SnH_4 at high pressure. This structure exhibits a $P6/mmm$ symmetry and is stable between 70 and 160 GPa. Because of the exceptionally strong EPC, very high superconducting temperatures are estimated. Low-frequency vibrations of massive Sn atoms and high-frequency vibrations of H_2 units are essential for the EPC [3]. Soft phonon modes have been observed and found to be very effective to enhance the EPC [24,25]. The soft phonon modes are induced by the FS nesting and Kohn anomalies. It is indeed remarkable that simple hydrides such as SnH_4 can achieve very high T_c at high pressures.

*Authors to whom correspondence should be addressed.
†Email address: John.Tse@usask.ca
‡Email address: yay451@mail.usask.ca

[1] C. Narayana *et al.*, Nature (London) **393**, 46 (1998).
[2] P. P. Edwards and F. Hensel, Nature (London) **388**, 621 (1997).
[3] N. W. Ashcroft, Phys. Rev. Lett. **92**, 187002 (2004).
[4] N. W. Ashcroft, J. Phys. Condens. Matter **16**, S945 (2004).
[5] J. Feng *et al.*, Phys. Rev. Lett. **96**,017006 (2006).
[6] L. Sun *et al.*, J. Phys. Condens. Matter **18**, 8573 (2006).
[7] Y. Yao *et al.* (to be published).
[8] Exploratory stimulated annealing calculations were performed using the SIESTA code [9] with Troullier-Martin pseudopotentials [10], double-zeta valence basis sets, and a smaller Monkhorst-Park (MP) [11] k-point set of $4\times4\times4$ on a supercell consisting of 20 SnH_4 units. Candidate structures were selected from the trajectory and then fully optimized with the VASP code [12] employing projected-augmented wave pseudopotentials [13] with a high-energy plane wave cutoff and a much larger k-point set.
[9] J. M. Soler *et al.*, J. Phys. Condens. Matter **14**, 2745 (2002); http://www.uam.es/departamentos/ciencias/fismateriac/siesta/.
[10] N. Troullier and J. L. Martins, Phys. Rev. B **43**, 1993 (1991).
[11] H. J. Monkhorst and J. D. Park, Phys. Rev. B **13**, 5188 (1976).
[12] G. Kresse and J. Furthmüller, Comput. Mater. Sci. **6**, 15 (1996).
[13] G. Kresse and D. Joubert, Phys. Rev. B **59**, 1758 (1999).
[14] A. D. Becke and K. E. Edgecombe, J. Chem. Phys. **92**, 5397 (1990).
[15] The electronic structure, lattice dynamics, and EPC have been investigated using the plane wave pseudopotential method, within the framework of perturbative density functional theory [16]. The electronic wave function and the charge density were expanded with a kinetic energy cutoff of 40 and 800 Ryd, respectively. The electronic band structure and DOS were computed with a $24\times24\times30$ MP mesh. Individual phonon calculations were performed on a $6\times6\times8$ MP mesh with a $12\times12\times16$ MP mesh for the first Brillouin zone (BZ) integrations. The EPC has been calculated in the first BZ on a $4\times4\times5$ MP q-point mesh using individual EPC matrices obtained with a $24\times24\times30$ k-point mesh. The convergence in the plane wave basis set and k-point sampling has been carefully examined by employing higher kinetic energy cutoffs and denser k-point sets. The accuracy of the interpolation was examined by comparing the results with phonon frequencies computed directly at selected q points.
[16] S. Baroni *et al.*, Rev. Mod. Phys. **73**, 515 (2001).
[17] A. Simon, Angew. Chem., Int. Ed. Engl. **36**, 1788 (1997).
[18] D. Kasinathan *et al.*, Phys. Rev. Lett. **96**, 047004 (2006).
[19] M. Wierzbowska, S. de Gironcoli and P. Giannozzi, cond-mat/0504077.
[20] J. M. An *et al.*, Phys. Rev. B **66**, 220502(R) (2002).
[21] P. B. Allen, Phys. Rev. B **6**, 2577 (1972).
[22] P. B. Allen and R. C. Dynes, Phys. Rev. B **12**, 905 (1975).
[23] P. B. Allen and R. C. Dynes, J. Phys. C **8**, L158 (1975).
[24] G. Profeta *et al.*, Phys. Rev. Lett. **96**, 047003 (2006).
[25] A. Yu. Ignatov, S. Y. Savrasov, and T. A. Tyson, Phys. Rev. B **68**, 220504(R) (2003).